COMMUNICATION

Resolving the backbone tilt of crystalline poly(3-hexylthiophene) with resonant tender X-ray diffraction

Received 00th January 20xx,
Accepted 00th January 20xx

DOI: 10.1039/x0xx00000x

Guillaume Freychet,[a] Paul Chantler,[b] Yuxuan Huang,[c] Wen Liang Tan,[b] Mikhail Zhernenkov,[a] Nagaraj Nayak,[d] Anil Kumar,[d] Peter A. Gilhooly-Finn,[e, f] Christian B. Nielsen,[e] Lars Thomsen,[g] Subhayan Roychoudhury,[h] Henning Sirringhaus,[c] David Prendergast,[h] and Christopher R. McNeill*[b]

The way in which conjugated polymers pack in the solid state strongly affects the performance of polymer-based optoelectronic devices. However, even for the most crystalline conjugated polymers the precise packing of chains within the unit cell is not well established. Here we show that by performing resonant X-ray diffraction experiments at the sulfur K-edge we are able to resolve the tilting of the planar backbones of crystalline poly(3-hexylthiophene) (P3HT) within the unit cell. This approach exploits the anisotropic nature of the X-ray optical properties of conjugated polymers, enabling us to discern between different proposed crystal structures. By comparing our data with simulations based on different orientations, a tilting of the planar conjugated backbone with respect to the side chain stacking direction of 30 ± 5° is determined.

Introduction

Conjugated polymers possess electronic and optical properties that make them suitable for application in polymer solar cells, light emitting diodes, transistors and thermoelectrics.[1-3] The pairing of optoelectronic properties typically found in inorganic semiconductors with physical properties associated with polymers provide conjugated polymers with unique qualities that are enabling low-cost, light-weight, mechanically flexible electronic devices. Many high performance conjugated polymers are semicrystalline, and it is well-established that the precise molecular-scale organization strongly affects the resulting semiconducting properties such as charge carrier mobility.[4] Our ability to determine the molecular packing of conjugated polymer chains, even in crystalline domains is limited. While the packing of small molecule organic semiconductors can be precisely determined by measuring single crystals with X-ray diffraction and applying so-called direct methods, conjugated polymers possess a degree of disorder that prohibits such an approach. Even for the most ordered semicrystalline conjugated polymers there are not enough diffraction peaks for proper refinement of the crystal structure.[5] Moreover, conjugated polymers can exhibit multiple low energy polymorphs that complicates analysis.[6]

The packing of semicrystalline conjugated polymer thin films has been studied with electron microscopy and X-ray diffraction techniques,[7-9] though the useful information extracted from diffraction studies is typically limited to the dimensions of the unit cell and the orientation of crystallites with respect to the substrate. Recently we demonstrated the potential of resonant X-ray diffraction experiments for unlocking information about the molecular organization of conjugated polymer chains within the unit cell.[10] Resonant diffraction exploits energy-dependent modulations of X-ray diffraction intensity as the X-ray energy is scanned across an elemental absorption edge.[11] Conjugated polymers are typically based on light elements such as carbon, oxygen and nitrogen which have absorption edges in the soft X-ray regime (~100 eV to 2000 eV); this limits their exploitation in resonant diffraction experiments due to their long wavelength. Many semiconducting polymers however contain sulfur as heteroatoms, with the sulfur K-edge located at ~2500 eV in the tender X-ray regime. This energy corresponds to a wavelength of ~0.5 nm which is small enough to permit interrogation of diffraction peaks corresponding to side chain stacking and backbone stacking. In our previous experiments we have demonstrated the ability of resonant X-ray diffraction at the sulfur K-edge to discern between different molecular conformers of the well-studied electron transporting polymer P(NDI2OD-T2).[10] We have also described how the anisotropic X-ray absorption properties of conjugated polymers such as P(NDI2OD-T2) result in highly anisotropic resonant diffraction

[a] NSLS-II, Brookhaven National Laboratory, Upton, NY 11973, USA.
[b] Department of Materials Science and Engineering, Monash University, Wellington Road, Clayton, Victoria, 3800, Australia.
[c] Cavendish Laboratory, University of Cambridge, JJ Thomson Avenue, Cambridge CB3 0HE, UK.
[d] Department of Chemistry, Indian Institute of Technology Bombay, Powai, Mumbai-400076, India.
[e] Department of Chemistry, Queen Mary University of London, Mile End Road, London E1 4NS, UK.
[f] Department of Chemistry, University College London, 20 Gordon Street, London, WC1H 0AJ, UK.
[g] Australian Synchrotron, ANSTO, 800 Blackburn Road, Clayton, Victoria, 3168, Australia
[h] The Molecular Foundry, Lawrence Berkeley National Laboratory, 1 Cyclotron Road, Berkeley CA 94720, USA.
Electronic Supplementary Information (ESI) available: [details of any supplementary information available should be included here]. See DOI: 10.1039/x0xx00000x

behaviour, with strong polarization dependent effects.[12] Furthermore, we have developed a numerical model that enables prediction of the resonant diffraction behaviour based on a given crystal structure enabling the predictions of molecular packing simulations to be directly compared with experiment. To summarise our progress with resonant tender X-ray diffraction so far, we have (i) shown how resonant diffraction can provide information about the *relative positions* of the resonant scatterers within the unit cell,[10] and (ii) described the strong anisotropy of resonant diffraction and how it can be understood in terms of the anisotropic atomic scattering factors.[12] In this contribution we show how the anisotropic scattering features can be interpreted which allows for a resolving of the titling of the conjugated backbone within the unit cell. This is analogous to angle-resolved NEXFAS spectroscopy[13] which can determine the tilt angle of molecules with respect to a substrate, except that here we are able to selectively interrogate the crystalline fraction of the sample, and determine a tilt angle with respect to the unit cell axes.

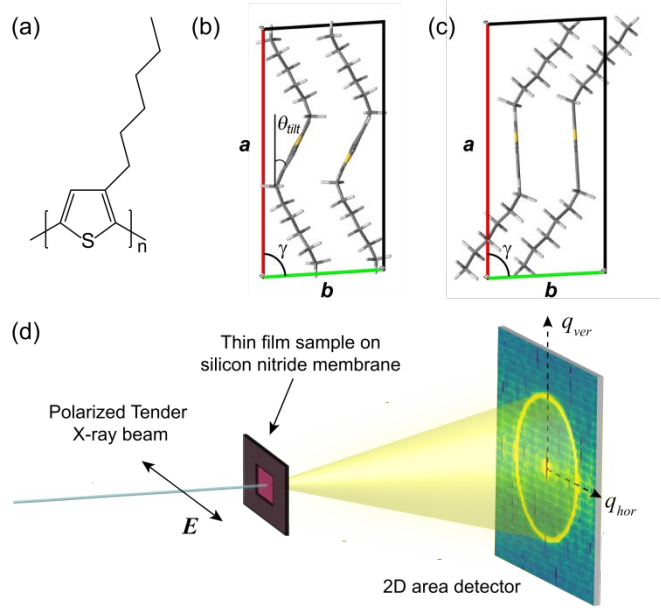

Fig. 1 (a) Chemical structure of P3HT. (b, c) Proposed unit cells looking down the ***c*** axis after Kayunkid et al.,[14] (b) and Dudenko et al.,[15] (c). The red line represents the ***a*** axis of the unit cell (side chain stacking) while the green line represents the ***b*** axis of the unit cell (π-π stacking). The angle γ is the angle between the ***a*** and ***b*** axes. (d) Schematic geometry of the transmission wide-angle X-ray scattering geometry used.

In this manuscript we also turn our attention to the most well-studied conjugated polymer, regioregular poly(3-hexylthiophene) (P3HT), see Fig. 1(a) for chemical structure.[16] P3HT has been studied for over 30 years in polymer solar cells,[17] field-effect transistors[18] and thermoelectrics.[19] Despite its performance in many of these applications being eclipsed by newer materials, it is still a relevant material and more recently has found application as the hole transport layer in efficient and stable perovskite solar cells.[20] Crystalline P3HT is known to exhibit different crystalline polymorphs.[21] Like most conjugated polymers, P3HT has a relatively planar conjugated backbone and pendant alkyl side chains. The main function of the pendant side chains is to enable solution processability, but these side chains also strongly influence the supramolecular organization of conjugated polymer chains. Due to the chemical incompatibility between the aliphatic side chains and conjugated backbones, P3HT assembles into layers of π-stacked backbones separated by layers of side chains. P3HT exists in two main crystalline forms distinguished by their side chain packing.[21] Form I is characterized by a larger side chain stacking distance of ~16 to 17 Å corresponding to non-interdigitated side chains. Form II has a much shorter side chain stacking distance of ~13 Å with interdigitated side chains.[22] Form I is found to form during the casting of thin films (as found in devices) while Form II requires special preparation conditions that promote the slow growth of crystals. Form I has thus been regarded as the kinetic product while Form II can be regarded as the thermodynamic product.[4]

Despite the importance of P3HT there is a lack of consensus regarding the exact unit cell packing of its crystalline forms. Even for Form I, there are different proposed structures which differ by their side chain angle, backbone tilt and relative position of adjacent backbones. Molecular mechanics/dynamics simulations of the solid state packing of P3HT indicate that the backbone adopts a planar all-trans conformation with extended side chains.[4, 23] A range of structural models have been proposed on the basis of the refinement of diffraction data often in combination with molecular modelling.[14, 15, 24-29] Two of the most refined models in terms of specifying precise locations for all atoms within the unit cell are given by Kayunkid et al.[14] and Dudenko et al.[15] who both propose that Form I of P3HT has a monoclinic unit cell with $P2_1/c$ space group and two chains per unit cell. Both models have similar unit cell dimensions of 16.0/16.3 Å (Kayunkid/Dudenko) for the *a* axis (side chain stacking direction), 7.8/7.7 Å for the *b* axis (π-stacking direction) and 7.8/7.6 Å for the *c* axis (backbone stacking direction), with γ = 86.5°/87.0° (see Fig. 1). With these unit cell parameters two polymer chains are accommodated along the *b* axis, along with two offset chemical repeats along the *c* axis. Although these two models propose similar unit cell parameters, the model of Kayunkid et al. has a substantially larger tilting of the polymer backbone within the unit cell (θ_{tilt}) compared to that of Dudenko et al., as shown in Fig. 1(b, c). The tilting of the conjugated backbone by ~ 25° with respect to the unit cell axes as proposed by Kayunkid et al. concurs with the findings of molecular dynamics simulations.[4, 23] A substantial tilting of the backbone was excluded however by Dudenko et al. on the basis of solid state NMR data, with a more recent crystal structure proposed by Yao et al. also having minimal backbone tilt.[29] It should be noted that the tilting of the backbones in the model of Kayunkid et al. is also accompanied by a lateral displacement of neighbouring thiophene rings which will have an impact on the charge transfer integral.[30] Hence these different crystal structures should result in different electronic properties.

The sensitivity of near-edge X-ray absorption events to bond-specific molecular orientation provides a fresh opportunity to probe tilting of the P3HT backbone within the unit cell. In a near-edge X-ray absorption fine structure (NEXAFS) spectroscopy experiment, the absorption strength corresponding to a specific electronic transition depends upon the orientation of the transition dipole moment with respect to the polarization of the incident X-ray beam.[13] The transition dipole moment for a given transition is determined by the geometry of the initial and final orbitals and has a specific orientation with respect to the molecular frame of the polymer backbone. While conventional NEXAFS spectroscopy can

measure the average tilt angle of the polymer backbone with respect to the substrate, it is equally sensitive to both amorphous and crystalline chains which limits its ability to specifically interrogate the crystalline phase.[31] Furthermore, thin film samples with a high degree of texture (preferential orientation of the unit cell axes with respect to the substrate) are also required. This same bond-orientation sensitivity however is encoded in energy dependent resonant diffraction data. Moreover, this energy dependence of resonant diffraction data is associated exclusively with the crystalline fraction of the sample giving resonant X-ray diffraction the potential to exclusively probe the molecular orientation of the P3HT backbone with respect to the unit cell axes.

In this paper, we describe the use of resonant X-ray diffraction at the sulfur K-edge in combination with first-principles calculations of X-ray absorption to resolve the molecular tilt of the polymer backbone in crystalline P3HT. These first-principles calculations enable us to determine the orientation of the transition dipole moments associated with the sulfur K-edge NEXAFS spectrum of P3HT with respect to the molecular frame of the P3HT backbone, and thus to establish the characteristic signature of the principal X-ray absorption spectra corresponding to polarization of the X-ray beam along the three orthogonal axes of the molecular frame. These simulations are then used to inform the reconstruction of the anisotropic atomic scattering factors from experiments. Comparing our experimental resonant diffraction data with simulated resonant diffraction profiles we find that a substantial tilting of the P3HT backbone is required to explain the experimental results.

Results and Discussion

Resonant diffraction experiments were performed on thin films in a transmission scattering geometry, see Fig. 1(d). Films were prepared by dissolving P3HT powder in chloroform and spin-coating onto glass substrates pre-coated with a water soluble sacrificial layer of sodium polystyrene sulfonate. Films were then typically annealed in a nitrogen glove box to 250 °C which is above the melting point and then slowly cooled at 1 °C per minute through the crystallization temperature. Melting was confirmed by a colour change from dark purple to bright orange, with the sample changing colour again to dark purple after recrystallization. After annealing, films were floated off in deionized water and transferred onto silicon nitride membranes. Films annealed at other temperatures were also studied, though melt-annealing improved the signal intensity due to an increased degree of crystallinity and stronger in-plane scattering intensity which is important for transmission experiments. The characteristic side chain spacing derived from the position of the (100) peak for all samples were similar at ~ 17 Å consistent with Form I packing. Batches of P3HT with different molar mass were also studied with further experimental details and experimental results provided in the Electronic Supplementary Information (ESI).

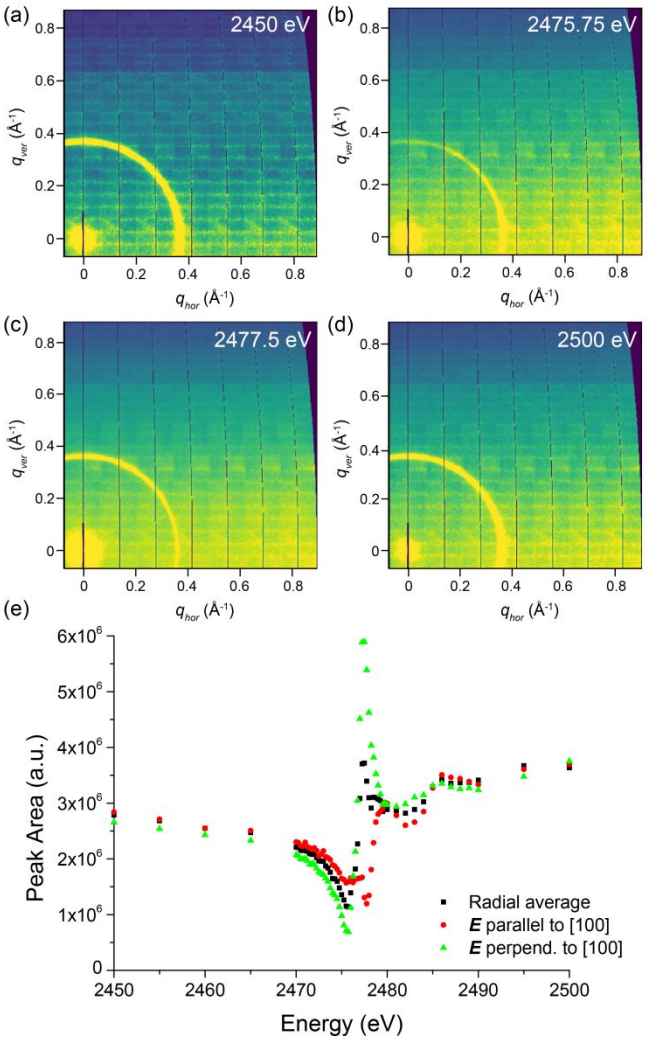

Fig. 2 (a) to (d): Two-dimensional WAXS patterns taken at (a) 2450 eV, (b) 2475.75 eV, (c) 2477.5 eV and (d) 2500 eV. (e) Energy dependence of the diffraction intensity of the (100) peak across the sulfur K-edge. Black squares represent the radially averaged diffraction intensity. The red circles represent diffraction intensity along q_{hor} corresponding to the electric field vector *E* being parallel to the side chain stacking direction. The green triangles represent diffraction intensity along q_{ver} corresponding to the electric field vector *E* being perpendicular to the side chain stacking direction.

Fig. 2 presents typical resonant diffraction data obtained for a 500 nm thick melt-annealed film with molar mass of M_n = 10 kg/mol, $Đ$ = 1.6 and a regioregularity greater than 98%. This batch of P3HT was produced by BASF (P200) and appears to be identical to one of the batches studied by Dudenko et al.[15] Although this film is relatively thick, X-ray absorption by the film is less than 5% and we do not observe any significant variation in our data for different film thicknesses (see ESI). Parts (a) to (d) in Fig. 2 show example transmission wide-angle X-ray scattering (WAXS) patterns taken at different energies across the sulfur K-edge. (Note that throughout this manuscript the reported energy values are in terms of the SMI beamline energy; compared with calibrated spectra taken at the Soft X-ray beamline at the Australian Synchrotron all energy values are shifted higher by about 4 eV.) A single peak is seen at ~ 0.36 Å^{-1} which corresponds to the (100) side chain stacking peak of "face-on" oriented chains. Grazing incidence WAXS patterns of

this sample can be found in the ESI. As the X-ray energy is scanned across the sulfur K-edge from 2450 eV (below) to 2500 eV (above) changes in the diffraction intensity and background intensity are observed. An increase in background intensity is seen crossing the sulfur K-edge due to an increase in X-ray fluorescence from the sample. The energy dependence of this background fluorescence enables us to measure a sulfur K-edge spectrum of the sample, as described previously.[10] Pronounced changes in the diffraction intensity of the (100) peak are also seen which are quantified by peak fitting. Fig. 2(e) plots the peak area of the (100) peak quantified by peak fitting that accounts for the varying background, based on 1-dimensional radially averaged line profiles, as well as for line profiles taken along the horizontal and vertical scattering directions. In addition to strong modulation of the diffraction intensity, we also observe pronounced diffraction anisotropy, with very different resonant diffraction profiles seen corresponding to diffraction in the horizontal direction and diffraction in the vertical direction. This diffraction anisotropy originates from the polarized X-ray beam (with the electric field vector (***E***) oriented in the horizontal direction) interacting differently with crystallites oriented with (100) direction parallel to ***E*** (corresponding to diffraction along q_{hor}) and crystallites oriented with (100) direction perpendicular to ***E*** (corresponding to diffraction along q_{ver}).[12] This diffraction anisotropy can also be seen in the 2D scattering patterns, with diffraction being more intense in the horizontal direction at an energy of 2475.75 eV (Fig. 2(b)), whereas diffraction is more intense in the vertical direction at an energy of 2477.5 eV (Fig. 2(c)). Below the absorption edge (i.e. at 2450 eV) and above (i.e. at 2500 eV) the diffraction intensity is equal along these two directions. The data of Fig. 2 is also provided as a Movie in the ESI. It is important to appreciate that due to the geometry of the experiment, diffraction observed along the q_{hor} direction arises exclusively from crystallites of P3HT with side chain stacking direction oriented parallel to ***E***, whereas diffraction observed along the q_{ver} direction arises exclusively from crystallites of P3HT with side chain stacking direction oriented perpendicular to ***E***. Thus although there is no macroscopic in-plane alignment of crystals in spin-coated samples, it is possible to separately measure diffraction from crystallites oriented with side chain stacking direction parallel and perpendicular to ***E***.

Spectroscopically, the resonant diffraction profiles shown in Fig. 2(e) are characterised by dips and peaks at different energies. For the radially averaged profile, there is a sharp minimum at 2475.5 eV and a sharp peak at 2477.5 eV with broader oscillations in intensity at higher energies. The resonant diffraction profile corresponding to diffraction with ***E*** parallel to the (100) direction is characterised by two minima at 2476 eV and 2477.5 eV, with similar oscillations at higher energies. The resonant diffraction profile corresponding to diffraction with ***E*** perpendicular to the (100) direction is characterised by a sharp minimum at 2475.5 eV and strong peak at 2477.5 eV. Thus these profiles corresponding to different orientations of the (100) direction relative to ***E*** are characterized by different spectroscopic features. Measurements on batches of P3HT with different molar mass also show the same spectroscopic features (see Fig. S3 in the ESI). In the following, these spectroscopic features will be related to different resonant transitions in P3HT and their associated anisotropic X-ray absorption properties.

To fully account for the anisotropic diffraction data of Fig. 2 requires knowledge of the anisotropic atomic scattering factors. The intensity of a particular reflection $\boldsymbol{h} = (h,k,l)$ is proportional to the square of the magnitude of the structure factor, i.e.,

$$I(\boldsymbol{h}) = |F(\boldsymbol{h})|^2 \quad (1)$$

The magnitude of the structure factor varies with energy due to the energy dependence of the atomic scattering factors:

$$F(\boldsymbol{h}) = \sum_j^{atoms} f_j \exp(2\pi i \boldsymbol{h}\cdot\boldsymbol{r}_j) \quad (2)$$

Here $\boldsymbol{r}_j$ is the position vector of the j^{th} atom in the unit cell (expressed in fractional coordinates) and f_j is the energy-dependent atomic scattering factor of the j^{th} atom. The intensity of a particular reflection thus depends on the strength of X-ray scattering from each atom as parameterized by f_j, and the relative position of the atoms in the unit cell along the (h,k,l) direction. The unit cell models of Kayunkid et al. and Dudenko et al., for example, provide atomic position data which can be used for $\boldsymbol{r}_j$, and thus with knowledge of f_j the resonant diffraction data can be computed. The output of calculations using different molecular models for $\boldsymbol{r}_j$ can then be compared with experiment.[10]

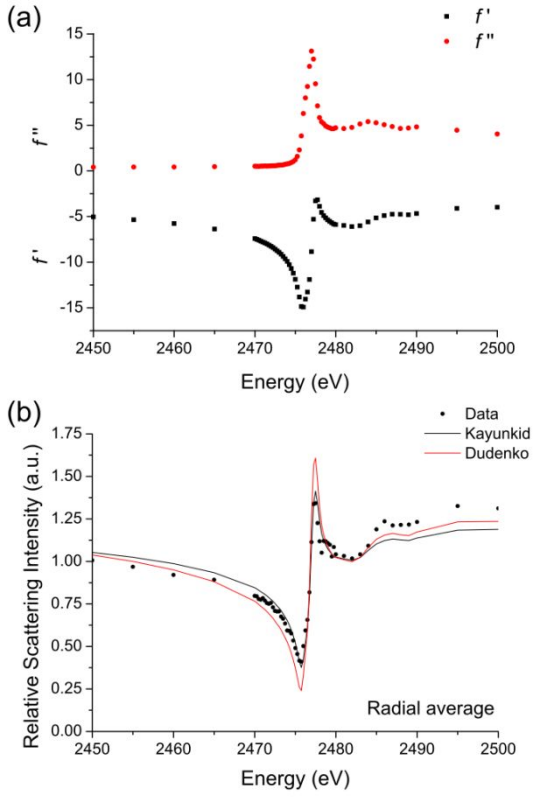

Fig. 3 (a) Atomic scattering factors f' and f'' of the sulfur atoms in P3HT based on fluorescence NEXAFS data from the resonant diffraction experiment on the spin-coated sample in Figure 2. (b) Comparison of the calculated resonant diffraction profiles based on the unit cell models of Kayunkid et al. and Dudenko et al. with the experimentally observed radially averaged (100) peak area. The simulations in part (b) were performed using the atomic scattering factors in part (a).

The atomic scattering factor *f* describes scattering of X-rays from an atom relative to that of a free electron. As well as being energy-dependent, the atomic scattering factor is complex and can be expressed as:

$$f = f_0 + f' + if'' \quad (3)$$

The term f_0 is independent of energy and can be approximated by the atomic number, reflecting the fact that a sulfur atom with 16 electrons will scatter 16 times more strongly than a single free electron (ignoring effects due to the bound nature of those electrons). Electrons in an atom however are bound, and cannot be simply treated as free electrons. In particular, close to X-ray absorption edges there are strong interactions between the incident X-ray beam and the electrons which are described by the energy-dependent term $f' + if''$. The imaginary part, f'', describes absorption by the sample and can be determined directly from X-ray absorption spectroscopy measurements. The energy-dependent real component, f', can then be determined via the Kramers-Kronig relationship.[32]

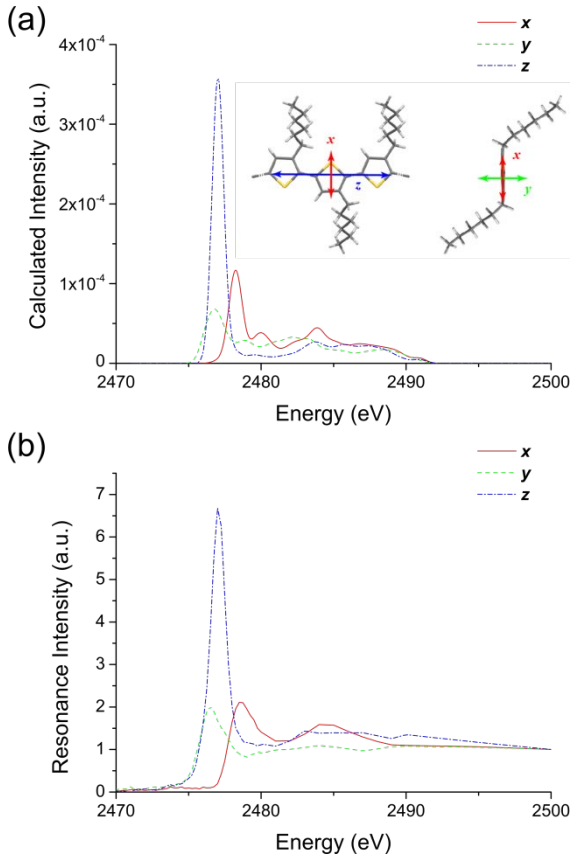

Fig. 4 (a) Results of first-principles calculations of the X-ray absorption spectra of P3HT for different orientations of the incident X-ray polarization relative to the frame of the planar conjugated backbone. The inset defines the axes of the molecular frame which have been used to define the principal axes of the backbone. These calculations were performed on crystalline P3HT using the Kayunkid unit cell. (b) Experimentally derived principal X-ray absorption spectra of P3HT for different X-ray polarizations.

For the carbon and hydrogen atoms in P3HT, tabulated values for *f* can be used as the X-ray energy is far enough away from any absorption edges. For the sulfur atoms in P3HT, *f* was determined from X-ray absorption spectroscopy measurements. For spin-coated samples such as those of Fig. 2, the NEXAFS spectrum derived from the fluorescence observed by the detector provides a spectrum that is radially averaged over all in-plane orientations. Fig. 3(a) shows the energy dependent radially averaged values of f' and f'' derived from the fluorescence data for the sample of Fig. 2. This data then enables calculation of the expected radially averaged resonant diffraction profiles corresponding to the models of Kayunkid et al. and Dudenko et al. The model of Kayunkid et al. predicts a stronger (100) diffraction intensity than that of Dudenko et al. by roughly a factor of two, see Fig. S6. However, since the observed diffraction intensity is not calibrated on an absolute scale, the predicted relative scattering profiles are compared to the experimental data in Fig. 3(b). Both predicted profiles were scaled to best fit the data using a least-squares approach. Better agreement (in terms of lowest sum-of-squares) is found between the data and the profile simulated using the model of Kayunkid et al., with χ^2 values of 0.20 for the Kayunkid model and 0.86 for the Dudenko model. In particular, the model of Dudenko et al. predicts a larger relative oscillation in the diffraction intensity than is experimentally observed. Although the Dudenko model better matches the data at higher energies, it is the resonant behaviour between 2470 eV and 2480 eV that is most sensitive to changes in the position of the resonant scatters (i.e. the sulfur atoms). The different predictions of the two models as shown in Fig. 3(b) are derived solely on basis of the relative positions of the sulfur atoms along the side chain stacking direction. The better agreement provided between the radially averaged data and the predictions of the Kayunkid model is the first indication that tilting of the molecular backbone provides a better explanation of the resonant diffraction data. Further scrutiny is provided by considering the full anisotropic scattering data, which requires knowledge of the anisotropic scattering factors.

To provide connection between the spectroscopic features observed with resonant diffraction and the underlying anisotropic molecular transitions at the sulfur K-edge, first-principles calculations of X-ray absorption[33] have been performed. Fig. 4(a) shows the calculated X-ray absorption profiles of crystalline P3HT (using the Kayunkid unit cell) corresponding to polarization of the X-ray beam oriented along the principal axes of the molecular frame of the polymer backbone. The inset to Fig. 4(a) defines the axes of the molecular frame, with ***x*** being oriented parallel to the thiophene ring plane but perpendicular to the backbone direction, ***y*** being oriented perpendicular to the thiophene ring plane, and ***z*** being oriented parallel to the backbone direction. The ability to define a coordinate frame for the P3HT backbone is enabled by the planar backbone of P3HT.

The three calculated X-ray absorption profiles are very distinct with spectroscopic features unique to each direction. Below 2480 eV each profile has a characteristic peak that is at a distinct photon energy. For polarization parallel to the ***x*** axis the dominant peak is at ~2478 eV with no strong resonances below this energy. For polarization parallel to the ***y*** axis the peak is located at 2476.5 eV, while for polarization parallel to the ***z*** axis

the peak is located at 2477 eV. The resonance at 2477 eV with polarization parallel to the backbone axis is particularly strong, consistent with previous observation that the dominant peak in the sulfur K-edge spectra of thiophene containing polymers is a 1s $\rightarrow$ σ* transition[12] rather than a 1s $\rightarrow$ π* which is typically found at the carbon K-edge.[31] First-principles calculations have also been performed on gas phase thiophene molecules which return qualitatively similar results in terms of dominant peaks and peak positions, see Fig. S7, however performing calculations on crystalline P3HT fully accounts for solid state effects. Calculations on crystalline P3HT using the Dudenko unit cell return similar results, see Fig. S8. Further details of the first-principles calculations are provided in the ESI.

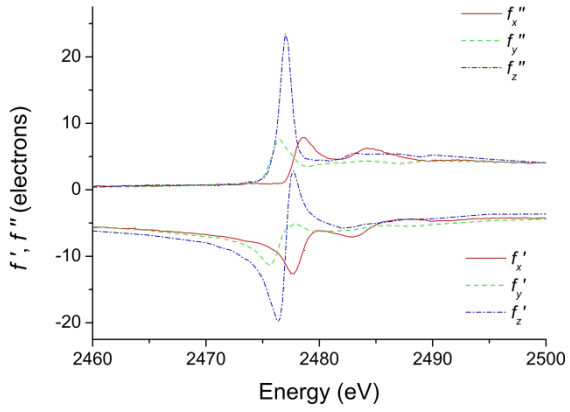

Fig. 5 Atomic scattering factors f' and f'' corresponding to orientation of the X-ray polarization along the three principal axes of the coordinate frame of the planar conjugated backbone.

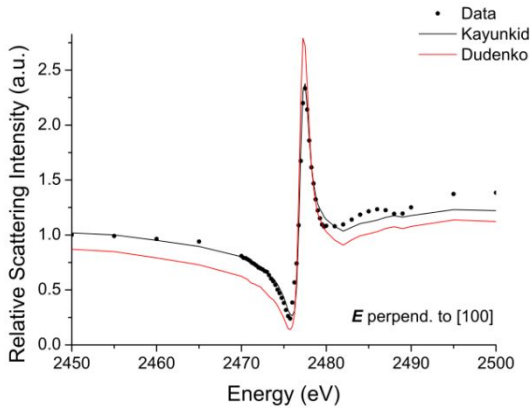

Fig. 6 Comparison of the calculated resonant diffraction profiles based on the unit cell models of Kayunkid et al. and Dudenko et al. with the data for the case when the X-ray polarization is perpendicular to the side chain stacking direction.

Fig. 4(b) presents experimentally derived X-ray absorption spectra of P3HT along the three principal molecular axes, ***x***, ***y***, and ***z***. These spectra were determined by measuring angle-resolved spectra of highly aligned films (prepared by mechanical rubbing) and edge-on oriented spin-coated films, with full details provided in the ESI. In short, as the ***z*** axis aligns with the polymer backbone direction, a spectrum with ***E*** preferentially aligned with ***z*** can be acquired by measuring a highly aligned sample with X-ray polarization parallel to the rubbing direction. For the ***x*** direction, angle-resolved spectra of edge-on oriented films were measured as a function of polar angle, with the contribution along the ***x*** direction greatest at grazing angles. A difference spectrum was calculated by comparing spectra at normal and grazing angles which was then used to extrapolate the measured spectrum until the unique spectrum shown in Fig. 4(b) was obtained with zero resonance intensity at 2477 eV and below. The remaining ***y*** spectrum was generated based on the principle that the three component spectra should sum to reproduce a spectrum acquired at the so-called "magic angle."[13] There is good consistency between the experimentally derived and simulated spectra. In particular, the ***z*** spectrum has a dominant characteristic peak at 2477 eV, with the ***y*** spectrum having its characteristic peak at a lower energy (2476.5 eV). Furthermore, the ***x*** spectrum has a distinct peak at higher photon energy (2478.5 eV) with zero resonance intensity at lower energies where the other two spectra have their characteristic peaks. Note that the simulated spectra in Fig. 4(a) do not include absorption resulting from transitions from 1s orbitals to the vacuum which results in a step-edge like absorption profile that accounts for the intensity in the experimental curves at photon energies greater than 2490 eV that is not present in the calculated curves.

Fig. 5 presents the corresponding atomic scattering factors based on the X-ray absorption spectra shown in Fig. 4(b). As the ***z*** axis is perpendicular to the side-chain stacking direction, f_z' and f_z'' can be directly used to calculate resonant diffraction profiles corresponding to the case when the polarization of the X-ray beam is perpendicular to the side chain stacking direction (corresponding data are the green triangles in Fig. 2(e)). Fig. 6 compares the calculated scattering profiles with the data with ***E*** perpendicular to the side chain stacking direction. Excellent agreement is found between the data and the simulations utilizing the atomic positions from the Kayunkid model. The Dudenko model again predicts a larger relative oscillation in the data than what is observed experimentally.

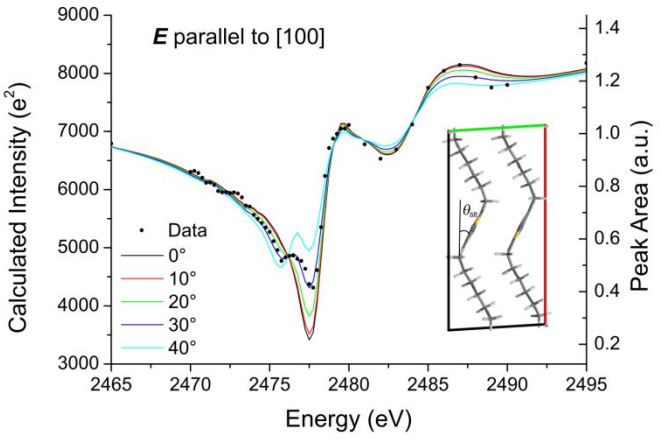

Fig. 7 Influence of backbone tilt angle θ_{tilt} on the calculated resonant diffraction profiles with comparison to data for the case when the X-ray polarization is parallel to the side chain stacking direction.

To reproduce the anisotropic resonant diffraction profile observed with ***E*** parallel to the side chain stacking direction, it is necessary to consider the possibility that the molecular axis ***x***

does not line up with the side-chain stacking direction [100]. In the case of the Dudenko unit cell, these two directions are parallel, and hence the observed scattering profile (red circles in Fig. 2(e)) should be accurately reproduced using f_x' and f_x'' from Fig. 5. However poor agreement is seen between the spectroscopic features seen in the data and the predictions based on a lack of backbone tilt. Fig. 7 compares the observed data (here the data presented is averaged over multiple data sets to improve the signal to noise ratio) with simulations using different molecular tilts of the backbone with respect to the unit cell axes. The data is characterized by two dips in the near-edge region, a smaller one at 2476 eV and a larger one at 2477.5 eV. The atomic scattering factors f_x' and f_x'' are unable to reproduce the dip at 2476 eV and predict a stronger dip at 2477.5 eV than is observed experimentally. Spectroscopically, the dip at 2476 eV is associated with the ***y*** spectrum while the dip at 2477.5 eV is associated with the ***x*** spectrum. By combining linear combinations of these two spectra in the right proportion (and determining the corresponding atomic scattering factors), the resonant diffraction profile can be calculated based on different tilting of the molecular frame relative to the unit cell. Fig. 7 compares the calculated resonant diffraction profiles as a function of backbone tilt angle, θ_{tilt}, with the experimental data. Varying the tilt angle brings about a continuous change in the relative prominence of these two spectroscopic features, with a value of θ_{tilt} = 30 ± 5° based on how closely the simulations match to the data. This angle is in good agreement with the value of 26 ± 5° reported by Kayunkid et al. and rules out the model of Dudenko et al. that has no backbone tilt. Note that atomic positions from the Kayunkid model were used in the calculations of Fig. 7. To check for how sensitive the calculations are to the exact atomic positions used, the calculations were repeated but using the atomic positions of the Dudenko model. A similar outcome was achieved (see Fig. S18) with a tilt angle of θ_{tilt} = 30 ± 5° again spectroscopically inferred. This observation indicates that the effects due to the anisotropic X-ray properties are able to more clearly distinguish between these two models as opposed to the effects due to the variations in the atomic positions. Note that our results do not prove the Kayunkid model, as we missing results for the (0k0) and (00l) directions and so cannot test the atomic position information along these directions. The (020) and (002) peaks are not accessible at the sulfur K-edge (the structure factor of the (010) and (001) peaks are zero), however resonant diffraction of poly(3-hexyl)selenophene[34] at the selenium K-edge is an intriguing possibility. Thus there could be other valid structures with a similar backbone tilt that would agree with our data, but they would also have to agree with other diffraction data on P3HT.

By understanding and exploiting the anisotropic X-ray optical properties of P3HT which relate to the molecular frame of the planar polymer backbone, we have shown that resonant X-ray diffraction is able to unambiguously resolve the tilting of the P3HT backbone within the unit cell. This approach will work for any sulfur-containing crystalline polymer with planar conjugated backbone, or planar subsection of the backbone that exclusively contains sulfur. For example, even though the polymer P(NDI2OD-T2) does not have a planar backbone,[35] the two thiophene units are co-planar allowing interrogation of the tilting of these thiophene units with respect to the unit cell axes. Indeed, the resonant diffraction profile of P(NDI2OD-T2) with ***E*** parallel to the side chain stacking direction also shows two characteristic near-edge dips, but in this case with the lower energy dip at 2476 eV being more prominent than the dip at 2478 eV.[12] Based on the observations here, a stronger dip at 2476 eV would indicate a larger tilting of the thiophene units in the unit cell of P(NDI2OD-T2) as compared to P3HT. For polymers without an appropriate heteroatom for resonant tender X-ray analysis, chemical labelling for example via chlorination (the Cl K-edge is at ~ 2800 eV) could provide a means of probing molecular orientation within the unit cell. In such a case, the X-ray absorption would be expected to be strongest with ***E*** aligned parallel to the C-Cl bond axis. For polymers without a planar backbone, judicious chemical labelling of a subsection of the backbone could also permit analysis of the molecular orientation of said subsection within the unit cell. It is increasingly common for high performance donor polymers used in polymer solar cells to contain multiple heteroatoms[36, 37] which could permit the use of multiple edges to separately probe the molecular orientation of subsets of the backbone.

Conclusions

The combination of resonant tender X-ray diffraction studies and first-principles calculations of X-ray absorption provide a new way to probe the molecular orientation of planar backbones within the unit cell of semicrystalline conjugated polymers. With knowledge of the anisotropic X-ray optical properties of the polymer backbone, the observed anisotropic resonant diffraction profiles can be interpreted. For Form I of crystalline P3HT studied here, a tilting of the planar backbone of 30 ± 5° with respect to the side chain stacking direction was determined, in agreement with the unit cell proposed by Kayunkid et al.

Acknowlegments

This research used the Soft Matter Interfaces (SMI) beamline (Beamline 12-ID) of the National Synchrotron Light Source II, a U.S. Department of Energy (DOE) Office of Science User Facility operated for the DOE Office of Science by Brookhaven National Laboratory under Contract DE-SC0012704. Work at the Molecular Foundry was supported by the Office of Science, Office of Basic Energy Sciences, of the U.S. Department of Energy under Contract No. DE-AC02-05CH11231. This work was also conducted in part at the Soft X-ray and SAXS/WAXS Beamlines at the Australian Synchrotron, part of ANSTO. HS acknowledges financial support from the European Research Council for a Synergy grant SC2 (no. 610115) and from the Engineering and Physical Sciences Research Council (EP/R031894/1). The authors thank Martin Brinkmann (CNRS)

and Vincent Lemaur (University of Mons) for discussions and sharing unit cell data.

Conflicts of interest

There are no conflicts to declare.

Notes and references

1. A. Facchetti, *Chem. Mater.*, 2011, **23**, 733-758.
2. R. H. Friend, R. W. Gymer, A. B. Holmes, J. H. Burroughes, R. N. Marks, C. Taliani, D. D. C. Bradley, D. A. Don Santos, J. L. Brédas, M. Lögdlund and W. R. Salaneck, *Nature*, 1999, **397**, 121-128.
3. B. Russ, A. Glaudell, J. J. Urban, M. L. Chabinyc and R. A. Segalman, *Nat. Rev. Mater.*, 2016, **1**, 16050.
4. Y. Olivier, D. Niedzialek, V. Lemaur, W. Pisula, K. Müllen, U. Koldemir, J. R. Reynolds, R. Lazzaroni, J. Cornil and D. Beljonne, *Adv. Mater.*, 2014, **26**, 2119-2136.
5. P. Brocorens, A. Van Vooren, M. L. Chabinyc, M. F. Toney, M. Shkunov, M. Heeney, I. McCulloch, J. Cornil and R. Lazzaroni, *Adv. Mater.*, 2009, **21**, 1193-1198.
6. A. Zhugayevych, O. Mazaleva, A. Naumov and S. Tretiak, *J. Phys. Chem. C*, 2018, **122**, 9141-9151.
7. D. M. DeLongchamp, R. J. Kline, D. A. Fischer, L. J. Richter and M. F. Toney, *Adv. Mater.*, 2011, **23**, 319-337.
8. A. Salleo, R. J. Kline, D. M. DeLongchamp and M. L. Chabinyc, *Adv. Mater.*, 2010, **22**, 3812-3838.
9. M. Brinkmann, *Mater. Chem. Front.*, 2020, **4**, 1916-1929.
10. G. Freychet, E. Gann, L. Thomsen, X. Jiao and C. R. McNeill, *J. Am. Chem. Soc.*, 2021, **143**, 1409-1415.
11. J.-L. Hodeau, V. Favre-Nicolin, S. Bos, H. Renevier, E. Lorenzo and J.-F. Berar, *Chem. Rev.*, 2001, **101**, 1843-1868.
12. G. Freychet, E. Gann, M. Zhernenkov and C. R. McNeill, *J. Chem. Phys. Lett.*, 2021, **12**, 3762-3766.
13. J. Stöhr, *NEXAFS Spectroscopy*, Springer, Berlin, 1992.
14. N. Kayunkid, S. Uttiya and M. Brinkmann, *Macromolecules*, 2010, **43**, 4961-4967.
15. D. Dudenko, A. Kiersnowski, J. Shu, W. Pisula, D. Sebastiani, H. W. Spiess and M. R. Hansen, *Angew. Chem. Int. Ed.*, 2012, **51**, 11068-11072.
16. S. Ludwigs, ed., *P3HT Revisited – From Molecular Scale to Solar Cell Devices*, Springer, 2014.
17. M. T. Dang, L. Hirsch and G. Wantz, *Adv. Mater.*, 2011, **23**, 3597-3602.
18. H. Sirringhaus, P. J. Brown, R. H. Friend, M. M. Nielsen, K. Bechgaard, B. M. W. Langeveld-Voss, A. J. H. Spiering, R. A. J. Janssen, E. W. Meijer, P. Herwig and D. M. de Leeuw, *Nature*, 1999, **401**, 685-688.
19. Q. Zhang, Y. Sun, W. Xu and D. Zhu, *Energy Environ. Sci.*, 2012, **5**, 9639-9644.
20. E. H. Jung, N. J. Jeon, E. Y. Park, C. S. Moon, T. J. Shin, T.-Y. Yang, J. H. Noh and J. Seo, *Nature*, 2019, **567**, 511-515.
21. M. Brinkmann, *J. Polym. Sci. B Polym. Phys.*, 2011, **49**, 1218-1233.
22. K. Rahimi, I. Botiz, N. Stingelin, N. Kayunkid, M. Sommer, F. P. V. Koch, H. Nguyen, O. Coulembier, P. Dubois, M. Brinkmann and G. Reiter, *Angew. Chem. Int. Ed.*, 2012, **51**, 11131-11135.
23. O. Alexiadis and V. G. Mavrantzas, *Macromolecules*, 2013, **46**, 2450-2467.
24. J. Mårdalen, E. J. Samuelsen, O. R. Gautun and P. H. Carlsen, *Solid State Commun.*, 1991, **80**, 687-689.
25. T. J. Prosa, M. J. Winokur, J. Moulton, P. Smith and A. J. Heeger, *Macromolecules*, 1992, **25**, 4364-4372.
26. S. Hugger, R. Thomann, T. Heinzel and T. Thurn-Albrecht, *Colloid Polym. Sci.*, 2004, **282**, 932-938.
27. Z. Wu, A. Petzold, T. Henze, T. Thurn-Albrecht, R. H. Lohwasser, M. Sommer and M. Thelakkat, *Macromolecules*, 2010, **43**, 4646-4653.
28. A. Bohle, D. Dudenko, N. Koenen, D. Sebastiani, S. Allard, U. Scherf, H. W. Spiess and M. R. Hansen, *Macromol. Chem. Phys.*, 2018, **219**, 1700266.
29. Z.-F. Yao, Q.-Y. Li, H.-T. Wu, Y.-F. Ding, Z.-Y. Wang, Y. Lu, J.-Y. Wang and J. Pei, *SmartMat*, 2021, **2**, 378-387.
30. V. Coropceanu, J. Cornil, D. A. da Silva Filho, Y. Oliver, R. Silbey and J. L. Brédas, *Chem. Rev.*, 2007, **107**, 926-952.
31. M. M. Nahid, E. Gann, L. Thomsen and C. R. McNeill, *Eur. Polym. J.*, 2016, **81**, 532–554.
32. B. Watts, *Opt. Express*, 2014, **22**, 23628-23639.
33. Y. Liang, J. Vinson, S. Pemmaraju, W. S. Drisdell, E. L. Shirley and D. Prendergast, *Phys. Rev. Lett.*, 2017, **118**, 096402.
34. M. Heeney, W. Zhang, D. J. Crouch, M. L. Chabinyc, S. Gordeyev, R. Hamilton, S. J. Higgins, I. McCulloch, P. J. Skabara, D. Sparrowe and S. Tierney, *Chem. Comm.*, 2007, DOI: 10.1039/B712398A, 5061-5063.
35. V. Lemaur, L. Muccioli, C. Zannoni, D. Beljonne, R. Lazzaroni, J. Cornil and Y. Olivier, *Macromolecules*, 2013, **46**, 8171-8178.
36. H. Chen, Z. Hu, H. Wang, L. Liu, P. Chao, J. Qu, W. Chen, A. Liu and F. He, *Joule*, 2018, **2**, 1623-1634.
37. R. Ma, T. Liu, Z. Luo, Q. Guo, Y. Xiao, Y. Chen, X. Li, S. Luo, X. Lu, M. Zhang, Y. Li and H. Yan, *Sci. China Chem.*, 2020, **63**, 325-330.